Combustion of nickel hyperaccumulator plants investigated by experimental and thermodynamic approaches

Laurent Cassayre, C. Hazotte, B. Laubie, W.M. Carvalho, M.-O. Simonnot

Combustion of nickel hyperaccumulator plants investigated by experimental and thermodynamic approaches

L. Cassayre[a,*], *C. Hazotte*[b], *B. Laubie*[b], *W.M. Carvalho Jr.*[a], *M.-O. Simonnot*[b]

[a] *Laboratoire de Génie Chimique, Université de Toulouse, CNRS, INP, UPS, Toulouse, France*
[b] *Université de Lorraine, CNRS, LRGP, 54000 Nancy, France*

Keywords:
Agromining
Phytomining
Nickel hyperaccumulator plant
Biomass combustion
Multiphase equilibrium calculations
Thermodynamics

A B S T R A C T

This work was undertaken to determine whether thermodynamic calculations can predict the amount and composition of ash produced by combustion of nickel hyperaccumulator (HA) plants in the context of agromining. To this end, three HA plants containing about 1 wt% of nickel were submitted to isothermal combustion at 550, 815, 900 °C and the solid residues were characterized by complementary techniques (TGA, XRD, ICP-OES, ion chromatography, SEM-EDX), while thermodynamic calculations were performed with the FactSage software using the dry biomass composition as input. We present an in-depth evaluation of inorganics behavior based on the combination and comparison of experimental data and calculations: effect of temperature on ash yield, nature of crystallized phases, ash elemental composition and inorganics volatilization. Our work confirms that equilibrium calculation is a powerful method to evaluate the behavior of inorganic elements during thermal treatment of biomass, despite some lacks in the databases. For the nickel HA plants, an innovative result is that, after combustion, nickel is always in the form of NiO particles, that can mix with MgO to form (Ni,Mg)O solid solutions. These results have direct implications for understanding the combustion process and for better design of the following leaching step aiming at Ni recovery.

1. Introduction

Agromining is a chain of processes that consists of cultivating hyperaccumulator (HA) plants to recover metals from soils, and extracting metals from plant tissues to obtain valuable products (van der Ent et al., 2015; Van der Ent et al., 2018). This environmentally friendly mining method relies on the ability of special plants, called HAs, to phytoextract metals from soils and store them in their above-ground parts, at concentrations of up to a few percent by mass. Agromining has been mainly developed for nickel (Ni), since huge areas of the world are covered with ultramafic Ni-rich soils. In 2015, more than 400 HA Ni plants have been documented worldwide, and new species have recently been discovered (Reeves et al., 2018). *Alyssum murale*, recently renamed *Odontarrhena muralis*, belonging to *Brassicaceae* family, has been extensively studied as a model plant for Ni agromining. Naturally present in several countries with temperate latitudes (*e.g.* Albania, Greece, Spain) and accumulating up to 1 wt% of Ni, its cultivation leads to the production of more than 100 kg of Ni per hectare (Bani et al., 2010; Chaney et al., 2018; Kidd et al., 2015; Pardo et al., 2018; Bani et al., 2015). Other plants in the same family are also of major interest, especially *Leptoplax emarginata*, able to reach higher Ni concentrations (Zhang et al., 2014). Trees of the *Violaceae* fam-

* *Corresponding author at*: Laboratoire de Génie Chimique, UMR 5503, 4 allée Emile Monso, CS 84234, 31 432 Toulouse cedex 4, France.
E-mail address: laurent.cassayre@ensiacet.fr (L. Cassayre).
https://doi.org/10.1016/j.cherd.2020.06.003

ily, such as *Rinorea bengalensis*, which grow in tropical areas, accumulate *ca* 3% of Ni in their leaves and are very promising (Reeves et al., 2018).

Various processes, mainly based on hydrometallurgy, have been designed to recover Ni from the aerial parts of *Brassicaceae*, the target synthetic compound being Ni ammonium and sulfate hexahydrate (Barbaroux et al., 2011; Barbaroux et al., 2009). Many other Ni compounds can also be produced. Most often, the first stage consists of burning the dry plant, in order to obtain ashes, which can be considered as a bio-ore: free of organic matter and containing up to 20 wt% of Ni. The chemical and structural nature of ash depends strongly on operating conditions, particularly temperature. Therefore, combustion is a key step, since the subsequent steps in the process are determined by the quality of the ash (Zhang et al., 2014; Houzelot et al., 2017). In addition, a Life Cycle Assessment study has shown that energy recovery is essential to reduce the environmental impacts of the overall agromining process (Rodrigues et al., 2016). The combustion stage has therefore been the subject of extensive experimental studies (Houzelot et al., 2017; Hazotte et al., 2019), with precise but time consuming analytical characterizations before and after combustion. In order to rationalize the understanding of the influence of the initial composition of the plants and of the operating conditions of combustion on the nature of the ashes, there is a need for numeric simulation.

In this work we have focused on computational thermodynamics, which has proven to be a powerful tool over the past decade to study the behavior of inorganics during biomass heat treatment such as gasification (Froment et al., 2013; Said et al., 2018; Kangas et al., 2014; Wan et al., 2018; Ma et al., 2015; Konttinen et al., 2013) and combustion (Stam and Brem, 2019; Becidan et al., 2009; Nordgren et al., 2013; Xing et al., 2018). Although the interest of equilibrium calculations is undeniable, two main difficulties remain in accurately describing these complex systems and processes. First, the establishment of reliable databases covering thousands of compounds and solutions remains a problem for the community, as mentioned by Lindberg et al. (2013), Konttinen et al. (2013) or Kaknics et al. (2015). Secondly, specific calculation procedures must be developed in order to take into account the specific non equilibrium behavior of organic matter during thermal treatment and its influence on the behavior of inorganics. In addition, industrial boilers and gasifiers are open systems in which the different material flows (such as inlet gas, flying ash, slags, tar, permanent gases) are not always in contact and subject to temperature gradients, which means that local equilibrium must be taken into account rather than global equilibrium. Depending on the specificity of the process, various calculation methods have been proposed (Said et al., 2018; Wan et al., 2018; Ma et al., 2015; Konttinen et al., 2013; Stam and Brem, 2019; Said et al., 2017; Thevenin et al., 2014).

The present work was undertaken to determine whether thermodynamic calculation enables us to predict the amount and composition of ash produced by combustion of HA plants, based on knowledge of their initial composition and operating temperature. For this purpose, three HA plants were selected and carefully characterized: (i) *Alyssum murale*, the "reference" plant, (ii) *Leptoplax emarginata*, potentially capable of accumulating higher amounts of Ni, and (iii) *Rinorea bengalensis*, of the *Violaceae* family. In order to overcome the above-mentioned problems related to industrial boilers, isothermal combustion was performed at 550, 815, 900 °C in a laboratory furnace, and the solid residues were characterized by complementary techniques. On the other hand, thermodynamic calculations were carried out, using the chemical composition of the three HA plants as an input. In this paper, we present an in-depth evaluation of ash composition, based on the combination and comparison of experimental data and thermodynamic calculations.

2. Materials and methods

2.1. Biomass

Alyssum murale plants were harvested at the flowering stage near Pogradec (Albania) on ultramafic soils containing 3–7 mg Ni per kg of dry soil (Bani et al., 2010). The aerial parts were sun-dried, and *ca* 500 kg were ground with an industrial grinder (SECOMI) up to a particle size of 2 mm. *Leptoplax emarginata* plants were harvested and sun-dried in an ultramafic area near the village of Eidián, 127 Ponteveda (Galicia, North-West Spain) (Kidd et al., 2018). The total concentration of Ni in soil was 861 mg kg^{-1}. They were ground in the laboratory using a blade grinder (Seb type 8100) to a particle size of 2 mm. Leaves of *Rinorea bengalensis* were collected from the Sabah Nature Park (Malaysia), on soils containing about 1000 mg kg^{-1} of Ni (van der Ent et al., 2017), and then sun-dried and ground with the same blade grinder to particle size of 0.1–0.4 mm. The moisture content of each plant was determined by weight loss after drying in an oven at 100 °C for 24 h.

In the rest of this article, these three plants are simply called *Alyssum*, *Leptoplax* and *Rinorea*.

2.2. Chemicals and reagents

The following chemicals were used for the chemical analyses: HNO_3 (≥65%) and H_2SO_4 (95–97%) provided by Sigma Aldrich, H_2O_2 (50%) by Alfa Aesar, HNO_3 Trace Metal Grade by Fisher Chemicals, and 64–69% Deionized (DI) water (Elga-Purelab Option).

2.3. Plant combustion

The combustion of each ground plant (*ca* 5 g) was performed in an electric furnace (Nabertherm, 30–3000 °C) at 550 and 900 °C, in air atmosphere. The temperature of 550 °C was chosen because (i) it is the conventional temperature of the ash yield determination for biomass since it is sufficient to degrade organic matter, and (ii) at this temperature there is no significant loss of inorganic volatile species (Koppejan and van Loo, 2012). The temperature of 900 °C is the estimated temperature reached in the boiler used for pilot combustion experiments (Houzelot et al., 2017). It can be noted that this temperature is in the low range of typical biomass combustion temperatures, which lie between 800 and 1100 °C depending on the type of biomass, according to Zeng et al. (2016).

The combustion was performed in conditions corresponding to the NF EN ISO 18122 standard for ash content determination. The temperature was increased to 250 °C at 6.25 °C min^{-1} and kept constant for 60 min; then, it was increased to 550 or 900 °C at 10 °C min^{-1} and kept constant for 120 min. The crucible was placed in a desiccator until temperature decreased to room temperature (20 °C) and the sample was weighed. These heating and cooling steps were repeated once, in order to verify that full calcination was reached. The whole procedure was repeated three times for each plant.

2.4. Analytical methods

2.4.1. Thermogravimetric analysis

The combustion of the ground plants was characterized by a thermogravimetric analysis (STAR^e system METTLER Toledo). Samples of *ca* 10 mg were placed in a standard alumina crucible (Al_2O_3, 70 μL) and heated from 30 to 1000 °C at 10 °C min^{-1}. The atmosphere was synthetic air containing 20% O_2 and 80% N_2, in volume (with H_2O < 3 ppm, CO < 1 ppm and CO_2 < 1 ppm), flushed at a flowrate of 50 mL min^{-1}.

The residual mass fraction measured by the analytical device, $r^{TGA}(T)$, is defined in Eq. (1).

$$r^{TGA}(T) = 100.\frac{m_{tot}^{TGA}(T)}{m_{tot}} \quad (1)$$

with:

$m_{tot}^{TGA}(T)$: measured total mass of the sample at temperature T,

m_{tot}: initial mass of the sample.

2.4.2. Chemical analyses

Solid samples of plants and ashes obtained by combustion were digested with 8.5 mL of HNO_3 and 1.5 mL of H_2O_2 in a microwave oven (Milestone Start D Microwave Digestion System), and filtered solutions were analyzed by ICP-AES (ICAP 6000 Series ICP Spectrometer). The analytical procedure (digestion and quantification) was validated by measuring a corn powder standard, V463 (USRAVE-INRA).

C, H, N and O were analyzed in all plants and ashes by CHNS-O Flash Analyser. The samples (1.5 mg) were used in a tin boat assortment for the percentage composition of C, H, N, while O was calculated by difference. These experiments were repeated 5 times at 960 °C. Calibration and quality controls were performed with sulfanilamide standard ($C_6H_8N_2O_2S$, Thermoscientific).

Additional analyses were carried out by the SOCOR certified laboratory, who measured ash amounts and elemental composition at 550 °C and 815 °C for the 3 plants. Furthermore, SOCOR laboratory performed chlorine concentration determination on the biomass, after solubilization by bomb combustion. The analytical technique was ion chromatography with a device (ICS 3000 Thermofisher Scientific Dionex) equipped with an IonPac AS18 column (4 mm x 250 mm) thermostated at 23 °C, using potassium hydroxide eluent.

2.4.3. Structural characterization

X-ray diffraction (XRD) analysis was carried out with the Discover D8 Advance Bruker X-Ray diffractometer, equipped with a Linxeyes detector (2θ–θ system) in the 2θ range from 3° to 63.3°, with a stepwise scanning of 0.03° and 5 s per step. The data were collected by XRD Commander software and processed with Crystallographica Search-Match software. Crystallographic phases were identified using the PDF-02 (Powder Diffraction File of International Center for Diffraction Data) database.

An estimate of the phase concentrations was calculated by correcting the scale factor with factor $I/I_{corundum}$. The scale factor is the overall multiplier factor of the standard peak intensities in order to optimize the matching of intensities. Factor $I/I_{corundum}$ is the relationship between the measured material intensity (I) and the Al_2O_3 corundum intensity ($I_{corundum}$) used as an internal standard during the standard measurement. This value is extracted directly from the database and used to quantify the concentration of each phase. This quantity gives an approximate measure of the mass fraction of the unknown that this standard represents. The concentration and $I/I_{corundum}$ values are only displayed for the matched materials for which $I/I_{corundum}$ is displayed in the database.

2.4.4. SEM-EDX characterization

The ash cross sections were prepared by embedding the powders in a non-conductive thermosetting resin (PolyFast, STRUERS) for hot molding (Mecapress 3, PRESI) and diamond polished to 1 μm (Mecatech 234, PRESI). Semi-quantitative cross-sectional analyses were carried out using a scanning electron microscope-field emission gun (SEM-FEG, JEOL JSM 7100F) equipped with an EDX Oxford ASDD X-Max detector.

2.5. Thermodynamic calculations

2.5.1. Calculation configuration

We used the Factsage 7.2 software (Bale et al., 2016) for equilibrium calculations. This program implements the method of total Gibbs energy minimization.

The initial system contains 100 g of biomass, with the three input compositions provided in Table 1, and air, whose composition is 21 O_2 and 79 N_2 (in mol%). 15 chemical elements are thus taken into account in this system. Since the experimental protocol consisted of heating a small amount of biomass in a laboratory furnace or TGA apparatus until the end of combustion, the equilibrium was computed with a large excess of air (air/biomass mass ratio of 500). The conditions are a constant total pressure (P_{tot} = 1 atm), while the temperature varies from 500 to 1000 °C in 25 °C steps.

We used a combination of compounds from the FactPS, FTOxid, FTSalt and FTmisc databases. As pointed out in the review of (Lindberg et al., 2013), a complete thermodynamic description of the liquid salt solution (Na^+, K^+, Ca^{2+}, Mg^{2+}//CO_3^{2-}, SO_4^{2-}, O^{2-}, Cl^-), which would have been relevant in this study, is not yet available. On the basis of preliminary calculations, our best compromise to represent the liquid solutions is based on the selection of three specific solutions, whose thermodynamic description is based on the Modified Quasichemical Model (Pelton and Chartrand, 2001):

- SLAGA, a liquid oxide solution phase including the major oxide compounds (Na_2O, K_2O, SiO_2, CaO, FeO, Fe_2O_3, MgO, ZnO, NiO, P_2O_5), considered as a single phase (no miscibility gap allowed);
- SALTB, a liquid molten chloride solution phase including oxides and hydroxides (K^+, Ca^{2+}, Na^+, Mg^{2+}, Ni^{2+}, Fe^{2+}//Cl^-, O^{2-}, OH^-), considered as a single phase (no miscibility gap allowed);
- LCSO, a liquid molten salt solution phase describing sulphate and carbonate mixtures of the two major inorganics contained in the biomass (K^+, Ca^{2+})//(CO_3^{2-}, SO_4^{2-}).

The choice of this last solution (LCSO) is based on the fact that sulphur forms liquid sulphate solutions under oxidizing conditions such as combustion, while it volatilizes as H_2S(g) under reducing conditions (Ma et al., 2015; Kaknics et al., 2015).

In addition, we considered an oxide solid solution containing (NiO, FeO, ZnO, MgO, CaO, Na_2O), which can form two phases (NiO and CaO base oxides, respectively) with partial

Table 1 – Elemental composition (average composition of 3 analyses, in wt%, normalized to 100%), ash yields and moisture content (average weight of 3 analyses, in wt%) of the 3 hyperaccumulator plants; σ: standard deviation.

Analytical technique	Element	Elemental composition of dry plant					
		Alyssum		*Leptoplax*		*Rinorea*	
		wt%	σ (%)	wt%	σ (%)	wt%	σ (%)
CHON	C	47.62	0.9	47.36	1.1	49.70	[a]
	H	5.18	0.1	6.25	0.2	6.53	[a]
	O	42.13	1.4	39.31	0.6	34.80	[a]
	N	1.24	0.3	1.68	0.1	1.76	[a]
ICP-AES	Ca	0.79	0.05	0.61	0.06	1.96	0.06
	Fe	0.04	0.02	0.03	0.01	0.00	0.00
	K	0.87	0.03	1.98	0.23	1.33	0.10
	Mg	0.15	0.01	0.19	0.04	0.59	0.01
	Na	0.05	0.01	0.04	0.01	0.02	0.00
	Ni	**1.06**	0.05	**0.59**	0.17	**1.46**	0.05
	P	0.23	0.01	0.22	0.03	0.09	0.00
	S	0.16	0.01	0.65	0.13	0.30	0.01
	Si	0.21	0.05	0.23	0.05	0.17	0.05
	Zn	0.01	0.00	0.00	0.00	0.01	0.00
Ion chromatography	Cl	0.26	[a]	0.85	[a]	1.30	[a]
Total before normalization (wt%)		96.6		94.4		94.0	
Moisture content (wt%)		8.94	0.17	8.49	1.71	8.02	[a]
Ash yield (wt%)	550 °C	7.28	0.09	9.23	0.15	11.35	[a]
	815 °C	11.1[b]	[a]	8.6	[a]	9.0	[a]
	900 °C	5.81	0.12	7.87	0.05	–	[a]

[a] Standard deviation is not provided when measurement is repeated only once.
[b] The ash yield for *Alyssum* at 815 °C was unexpectedly high and the measurement could not be repeated. This value was discarded in the rest of the article.

miscibility. Conversely, due to the lack of experimental data, the thermodynamic description of the CaO–K_2O and NiO–K_2O systems is very poor in these databases.

With the 15 elements taken into account in the calculations, the database combination leads to the inclusion of 283 gaseous species (the gaseous phase is considered an ideal mixture of all species), 3 liquid solutions (SLAGA, SALTB and LCSO), 464 solid compounds and 2 solid solutions (MeO_A#1 and MeO_A#2, representing the NiO and CaO base oxides).

2.5.2. *Data processing*

For each temperature step, the Equilibrium module of the Factsage software provides the amount of each stable phase (pure solids, solutions and gaseous species). The residual mass fraction of the condensed phases (*i.e.* the solid compounds and the solutions), $r_{tot}^{calc}(T)$, is defined in Eq. (2).

$$r_{tot}^{calc}(T) = \frac{100}{m_{tot}} \sum_{i=1}^{n(T)} m_i^{calc}(T) \quad (2)$$

with:

m_{tot}: initial mass of the system (100 g),

$m_i^{calc}(T)$: calculated mass of condensed compound/solution i at temperature T (g),

$n(T)$: number of stable phases (except the gas phase) at temperature T.

The value of $r_{tot}^{calc}(T)$ is directly compared to the experimental residual mass fraction of ashes determined either by weighing the cold ashes obtained in the laboratory furnace or by *in situ* recording during thermogravimetric analysis $r^{TGA}(T)$ (see Section 3.2).

The list of stable compounds is stored at each calculation step. The condensed phase assembly is then compared to XRD analysis of solid residues (see Section 3.3). Given the detection limit of XRD (usually around 5 wt%), compounds representing less than 1 wt% (*i.e.* compounds for which $m_i^{calc}(T) < 0.01\ r_{tot}^{calc}(T)$) are not considered in this comparison.

Eq. (3) defines the mass percentage $p_j^{calc}(T)$ of each of the 15 elements in the residue at temperature T. Since FactSage software does not provide this specific output, we have designed a specific macro file in order to calculate the elemental mass distribution at each temperature.

$$p_j^{calc}(T) = \frac{100}{m_{tot}^{calc}(T)} \sum_{i=1}^{n(T)} \frac{M_j}{M_i} m_i^{calc}(T) \quad (3)$$

with:

$p_j^{calc}(T)$: calculated mass percentage of element j in the residue at temperature T,

j: one of the 15 elements constituting biomass,

$m_{tot}^{calc}(T)$: calculated total mass of the residue,

M_j and M_i: molar mass of element j and compound/solution i.

The values of p_j^{calc} are then compared with the elemental analyses of the solid residues carried out after combustion (see Section 3.4).

Eq. (4) defines the proportion $v_j(T)$ (in %) of element j in the gas phase relative to the total quantity of j in the system at temperature T. This value provides an indication of the volatility of each element. It can be obtained directly from equilibrium calculations and deduced from the ash yield and elemental analyses of the solid residue (see Section 3.5).

$$v_j(T) = 100 \frac{m_j^{gas}(T)}{m_j^{tot}} \quad (4)$$

with:

$m_j^{gas}(T)$: mass of element j in the gas phase at temperature T,

m_j^{tot}: mass of element j in the initial biomass.

3. Results

A systematic comparison between the available experimental data (total mass, XRD analyses and elemental composition of solid residues) and thermodynamic calculations is presented in this section for the three HAs plants.

3.1. Biomass composition

The elemental composition of the three plants is given in Table 1. The raw data led to a mass balance of approximately 95% for each plant; the data provided in Table 1 were normalized to 100%.

The composition of *Alyssum* is similar to that determined by Barbaroux et al. (2012) and Hazotte et al. (2019). The amount of nickel reported by Guilpain et al. (2018) and Zhang et al. (2014) was lower (0.51 ± 0.07 wt.%), but the plants used for the experiments were not grown in the same year and on the same plot. As for *Rinorea*, our results (Ca, K, Mg, Ni) are very comparable to the concentrations measured by Guilpain et al. (2018).

Similarly to many other varieties of biomass, the main elements in the three HA plants are C > O > H > N (in decreasing order of abundance), and the major inorganics are Ca and K (Vassilev et al., 2013). The specificity is the high Ni content (between 0.59 and 1.46 wt%), this element being usually a trace element (<0.1 wt%) in biomass (Vassilev et al., 2013). Furthermore, each plant is chemically different: *Alyssum* is Ni rich (Ni > K > Ca), *Leptoplax* is K rich (K > Ca > Ni) and *Rinorea* is Ca rich (Ca > Ni > K). In addition, *Rinorea* is very rich in chlorine, with a K/Cl molar ratio smaller than unity, which is quite unusual for biomass. Finally, *Leptoplax* is the richer plant in S.

3.2. Effect of temperature on ash yield

Fig. 1 shows the measured amounts of TGA ash ($r_{tot}^{TGA}(T)$, defined in Eq. (1)) and combustion experiments, and the calculated mass fraction of the solid residue ($r_{tot}^{calc}(T)$, defined in Eq. (2)) between 500 and 1000 °C. It should be noted that the largest mass loss occurring between 200 and 480 °C (where the residual mass fraction decreases from 90% to about 10%), which corresponds to the combustion of organic elements, is not shown in Fig. 1 since our goal is focused on ash behavior.

For all plants, acceptable repeatability of TGA measurements is obtained, indicating satisfactory sample homogeneity. Indeed, the maximal difference (in absolute value) between two measurements is about 1% for *Rinorea*, and it is much lower for the two other plants. For each plant, the residual mass decreases with temperature and stabilizes at around 900 °C. The final residual mass is comparable for *Rinorea* and *Leptoplax* (7.9% and 7.5%, respectively) and significantly lower for *Alyssum* (4.6%). There are significant differences in the total mass loss measured between 500 and 1000 °C, since *Rinorea* loses about 4% of its initial mass in this temperature range, while *Leptoplax* and *Alyssum* lose 2% and 1% respectively. These mass losses result in a significant drop in mass at about 600–650 °C for *Alyssum* and *Rinorea*, while a second event is detected at about 800–850 °C for *Leptoplax* and *Rinorea*. This overall behavior indicates that several reactions are involved between 500 and 900 °C, with the formation of volatile compounds.

The weight of ash recovered after furnace experiments is very consistent with TGA measurements for *Leptoplax* and *Rinorea*. However, the ash yield determined for *Alyssum* by combustion in the furnace is significantly higher than the residual mass measured by TGA.

For the calculated residual mass, the overall picture is convincing: the influence of temperature and the amount at 900 °C (6.9%, 5.5% and 4.7% for *Rinorea*, *Leptoplax* and *Alyssum*, respectively) are consistent with the experimental results, and the mass drops measured at 600–650 °C and 800–850 °C are reproduced in the simulation. However, the equilibrium calculations clearly underestimate (by about 2% in absolute value) the ash yield for the 3 plants.

The results on phase assembly and elemental ash composition, presented in the next sections, will help us to discuss more specifically the influence of temperature on ash composition and the relevance of the thermodynamic calculations for understanding it.

3.3. Nature of the crystallized phases

A representative diffractogram of each solid residue obtained after combustion at 550 and 900 °C is shown in Fig. 2. A general observation is that there are large differences between each plant, and even between the two temperatures for a given plant. This illustrates the major importance of the initial composition of the biomass and the combustion temperature on the final composition of the residue.

Several remarks can be drawn from the diffractograms:

- Ni is present in each plant and at each temperature as a single phase of nickel oxide (NiO).
- K is involved in K_2SO_4 and KCl in ashes at 550 °C, and only in K_2SO_4 in ashes at 900 °C.
- Cl is not present in any crystallized phase at 900 °C.
- Si is involved in several silicate phases ($Ca_3MgSi_2O_8$, $CaMgSi_2O_6$, Ca_2SiO_4, Mg_2SiO_4).
- Hydroxyapatite $Ca_5(PO_4)_3(OH)$ is detected in almost all samples.
- Due to their low content in the initial HAs, the elements Fe, Na and Zn are not present in any phase identified by XRD.

The calculated quantity (in wt% of the solid residue) of each phase is compared to the phases identified by XRD in Table 2. For experimental XRD data, a distinction is made in the table between minor (m) phases, accounting for less than 10 wt% (determined with our quantification method described in Section 2.4.3), and major (M) phases (more than 10 wt%).

A relatively good correspondence between the simulation and the experimental XRD is obtained, since almost all major and minor phases identified in the diffractogram analyses are predicted by equilibrium calculations. In addition, most of the major phases of the experimental diffractograms correspond to phases that represent more than 15–20 wt% in our calculations. The only notable exception is the presence of calcium carbonate ($CaCO_3$) in *Alyssum* ashes, identified by intense diffraction peaks (Fig. 2a and b) but not present in the calculated phase assembly. As illustrated in the predominance diagram in Fig. SI1, the decomposition temperature of $CaCO_3$ under 0.21 atm of O_2 is 876 °C, and thus it is expected that, at 900 °C, $CaCO_3$ decomposes into CaO and CO_2(g).

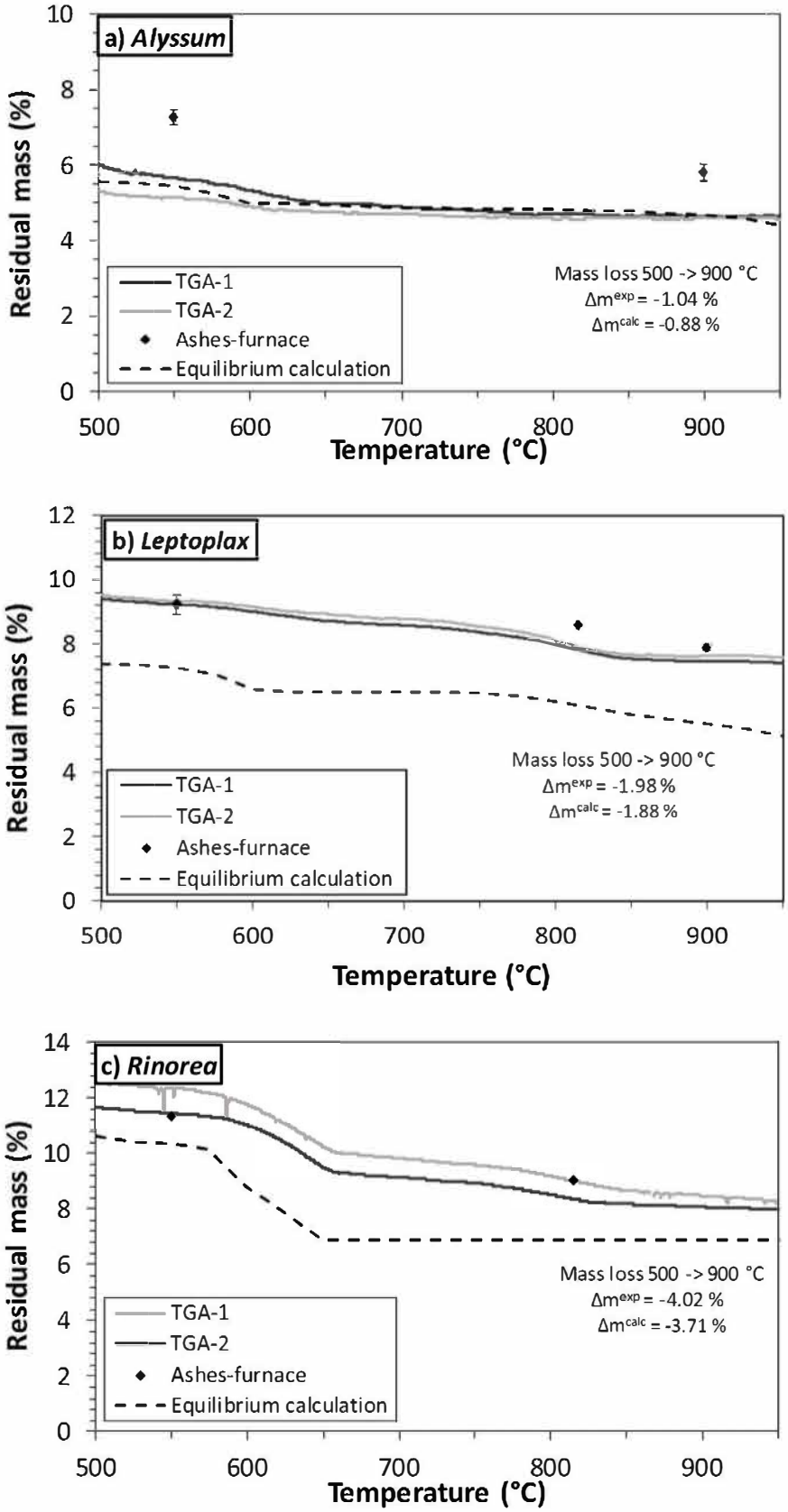

Fig. 1 – Influence of temperature on the amount of solid residue during combustion in air–comparison between thermogravimetric measurements, weighing of recovered ashes and equilibrium calculations for (a) *Alyssum*; (b) *Leptoplax*; (c) *Rinorea*.

It can also be noted that, with our selection of liquid solutions from the thermodynamic database, practically no liquid phase is expected to form at 550 or 900 °C, with the exception of 11 wt% of SLAGA for *Alyssum* combustion at 900 °C. Thus, the formation of liquid phases is not expected to have a strong influence on reactions during combustion up to 900 °C.

An important feature related to the analyses of the phases present in the ashes is that the calculation predicts the

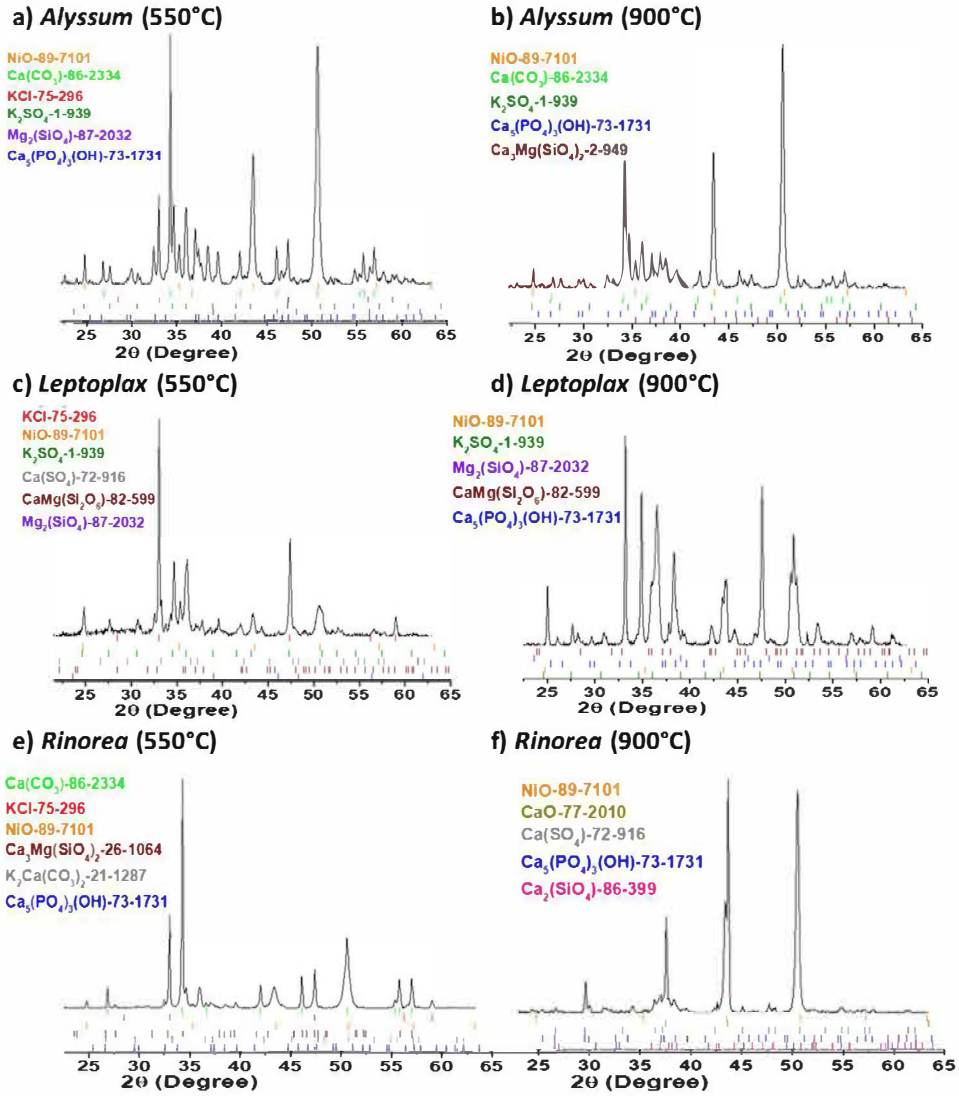

Fig. 2 – X-ray diffraction patterns of biomass ashes obtained by combustion at 550 °C and 900 °C of *Alyssum* (a and b), *Leptoplax* (c and d) and *Rinorea* (e and f). For each figure, the phases are listed in order of decreasing quantity, with their corresponding PDF file number.

formation of a (Ni,Mg)O phase for each plant and at each temperature, while XRD peaks are attributed to NiO. As for the result of the calculation, the MeO_A#1 phase is a complete solid solution between NiO and MgO, which means that if NiO and MgO are both present, they will mix in all proportions. With regard to the identification of diffraction peaks, it appears that NiO, MgO, and the mixed oxide ($Mg_{0.4}Ni_{0.6}O$) can hardly be distinguished since their diffraction peaks are located at the same angles (Fig. SI2). Thus, if equilibrium is reached, the NiO phase identified on each XRD might contain a significant proportion of MgO.

This aspect was confirmed by the additional SEM-EDX *in situ* cross sectional analysis of nickel oxide particles observed in HA ash, the representative results of which are compiled in Fig. 3. Indeed, we could demonstrate by point analysis the presence of 0–10 wt% of Mg (based on the metal) in nickel oxide particles from *Alyssum* ash burnt at 900 °C (Fig. 3a). For *Rinorea*, individual nickel oxide particles could not be analyzed due to their small size (about 1 μm or less), but the elemental mapping presented in Fig. 3b indicates that Ni element is systematically combined with Mg, which corresponds to the formation of the mixed oxide (Ni,Mg)O.

3.4. *Ashes elemental composition*

Fig. 4 shows the elemental composition of ash (in wt%) determined by (i) elemental analyses of ash recovered after combustion at 550, 815 and 900 °C, and (ii) thermodynamic calculations with a temperature step of 10 °C. For the three HAs, the evolution of the concentration of the major inorganic elements Ni, K, Ca, Mg and S is presented in the temperature range 500–1000 °C. It should be noted that the Cl content of the ashes was not determined due to the experimental difficulty of such an analysis; however, the behavior of this element will be discussed in the next section using thermodynamic prediction.

Due to the combustion of plants, most organic matter has volatilized. As a result, the concentrations of inorganics in ash are much higher than in the original plant and, as shown in Fig. 4, they are very variable depending on the nature of the plant. Ni content is about 18 wt% for *Alyssum* and *Rinorea*, and 8 wt% for *Leptoplax*.

For each HA plant, two combustion tests and subsequent elemental analyses were performed independently at 550 °C (one at LRGP, the other at SOCOR). Considering the relative dispersion of these analyses and the small variations in con-

Table 2 – Comparison between the phases in the solid residues from calculation and XRD analysis (M: major phase detected by XRD; m: minor phase detected by XRD).

Alyssum	550 °C			900 °C		
	Phase	wt% calc.	XRD	Phase	wt% calc.	XRD
	$Ca_5HO_{13}P_3$(s)	20.3	m	$Ca_5HO_{13}P_3$(s)	18.6	m
	$CaMgSi_2O_6$(s)	5.9	–	$Ca_3MgSi_2O_8$(s)	20.9	m
	$Ca_2MgSi_2O_8$(s)	16.3	–	K_2SO_4(s2)	16.3	M
	K_2SO_4(s)	15.6	m	$CaCO_3$(s)	–	M
	KCl(s)	8.0	M	$(Ni_{0.81}Mg_{0.14})O$[a]	32.7	M
	K_2CO_3(s)	4.7	–	SLAGA	11.5	–
	$CaCO_3$(s)	–	M			
	$(Ni_{0.82}Mg_{0.16}Fe_{0.02})O$[a]	27.7	M			
Leptoplax	550 °C			900 °C		
	Phase	wt% calc.	XRD	Phase	wt% calc.	XRD
	$Ca_5HO_{13}P_3$(s)	16.5	–	$Ca_5HO_{13}P_3$(s)	21.6	m
	Mg_2SiO_4(s)	3.9	m	Mg_2SiO_4(s)	3.3	m
	$CaMgSi_2O_6$(s)	8.3	m	$CaMgSi_2O_6$(s)	13.5	m
	K_2SO_4(s)	46.7	m	K_2SO_4(s2)	45.5	M
	$K_3Na(SO_4)_2$(s)	8.1	–	$(Ni_{0.79}Mg_{0.14}Fe_{0.04})O$[a]	15.9	M
	KCl(s)	10.6	M			
	$CaSO_4$(s)	–	m			
	$(Ni_{0.88}Mg_{0.09}Fe_{0.02})O$[a]	11.2	m			
Rinorea	550 °C			900 °C		
	Phase	wt% calc.	XRD	Phase	wt% calc.	XRD
	$Ca_5HO_{13}P_3$(s)	4.4	m	$Ca_5HO_{13}P_3$(s)	6.7	m
	Ca_2SiO_4(s)	10.3	m	Ca_2SiO_4(s)	15.5	m
	KCl(s)	23.1	M	$CaSO_4$(s)	18.2	m
	$CaCO_3$(s2)	21.8	M	$(Ni_{0.51}Mg_{0.49})O$[a]	41.1	M
	$CaSO_4$(s)	12.2	–	CaO[b]	18.5	M
	$(Ni_{0.51}Mg_{0.49})O$[a]	27.4	M			

[a] Composition of the MeO_A#1 solid phase.
[b] Composition of the MeO_A#2 solid phase).

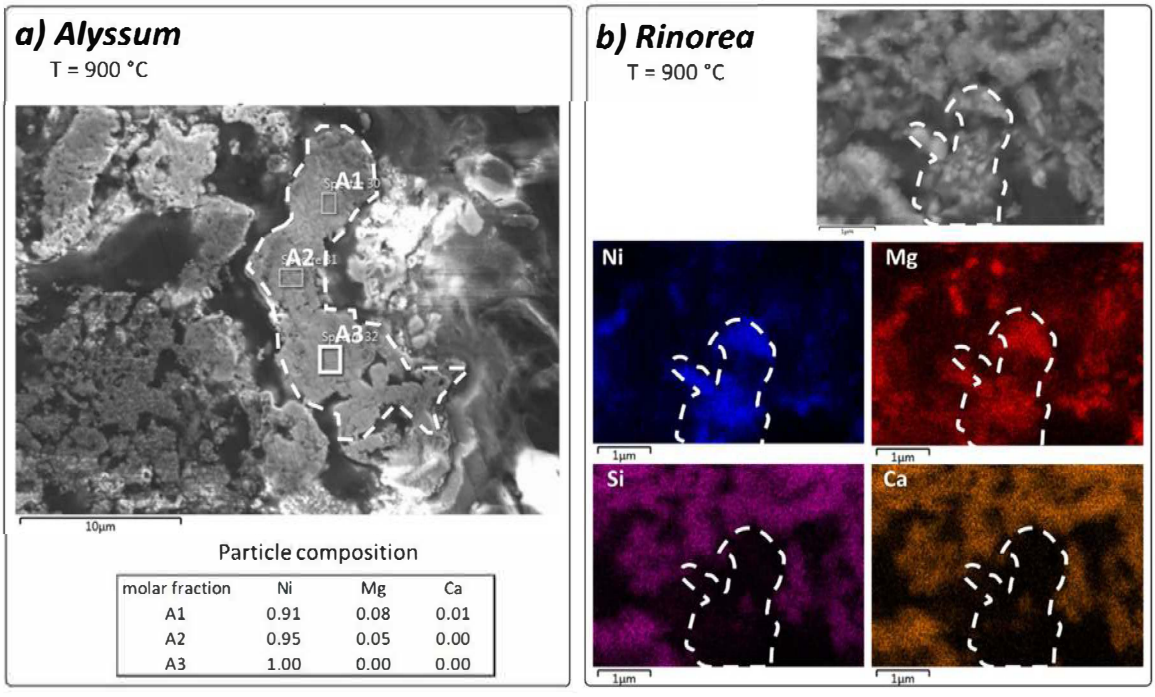

Fig. 3 – SEM-EDX analysis biomass ashes obtained by combustion at 900 °C (a) local composition (on metal basis) of a nickel oxide particle from *Alyssum* ashes; (b) local elemental mapping of a group of nickel rich particles from *Rinorea* ashes.

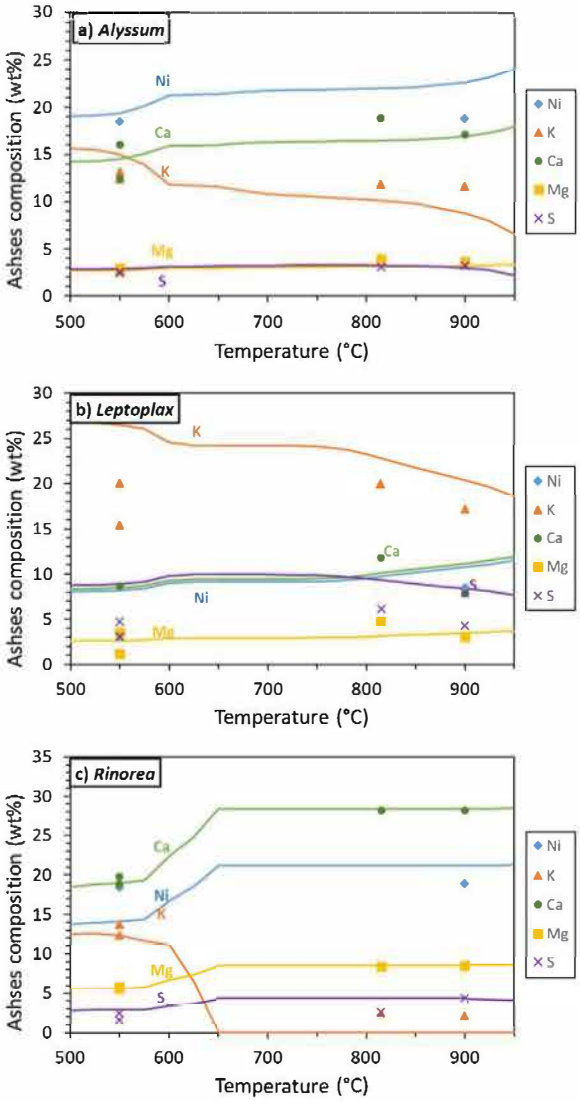

Fig. 4 – Influence of temperature on ashes elemental composition – comparison between ICP elemental analyses (symbols) and equilibrium calculations (lines) for (a) *Alyssum*; (b) *Leptoplax*; (c) *Rinorea*.

centration observed for *Alyssum* and *Leptoplax* (Fig. 4a and b), we consider that our experimental data only show a significant influence of the combustion temperature for *Rinorea* (Fig. 4c). This can be related to the TGA recordings (Fig. 1) which show a much higher mass loss for *Rinorea* in the temperature range of 500–900 °C. Of the elements shown in Fig. 4c, K is the only element whose concentration decreases (from about 13 wt% at 550 °C to 2 wt% at 815 and 900 °C), indicating that the overall mass loss is related to K-containing compounds. In relation, the concentration of the other elements (Ca, Ni, Mg and S) increases proportionally.

With regard to the simulations, there is again a global agreement between the experimental data and the equilibrium calculations. For *Alyssum* and *Rinorea*, the absolute concentration values and the influence of temperature are very consistent, and the calculation represents well the decrease in concentration of K in *Rinorea* ashes. An obvious difference concerns the amount of K in *Leptoplax* (Fig. 4b), which is largely overestimated at 550 °C by the simulation.

The specific case of carbon, whose amount was determined in *Alyssum* and *Leptoplax* ashes after combustion at 550 and 900 °C, is represented in Fig. 5. It comes that the increase of

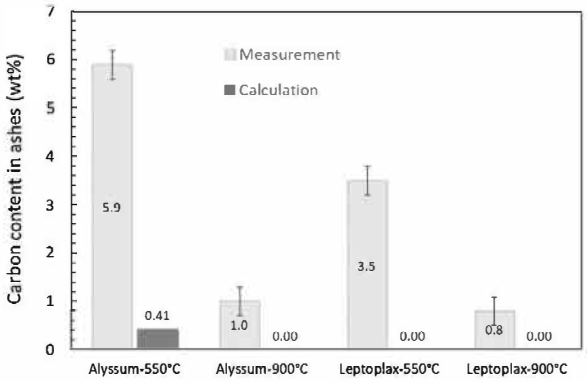

Fig. 5 – Carbon content in *Alyssum* and *Leptoplax* ashes at 550 and 900 °C.

combustion temperature strongly reduces the carbon content in the ashes, which is most likely due to the decomposition of carbonate phases such as $CaCO_3$. However, there is a noticeable discrepancy between the data and the calculations, since almost no carbon is foreseen in the solid residue. This point will be further discussed in Section 4.

3.5. *Volatilization of inorganics*

Fig. 6 compiles calculations based on the volatilization of elements from ashes. In Fig. 6a, c and e, the elemental fractions of K, Cl Na and S in the gas phase are plotted as a function of temperature for the 3 HAs, as defined in Eq. (4). The other inorganic elements (Zn, Ni, Fe, Ca, P, Si and Mg) remain entirely in condensed phases, most of which being listed in Table 2. The amount of K deduced from experimental data (ash yield and K content in ashes) is also plotted in these figures. Fig. 6b, d and f shows the speciation of the gas phase, *i.e.* the nature of the main stable gaseous compounds in the temperature range of 500 to 1000 °C.

For each plant, there is a strong difference between 550 °C, with almost no volatilization of inorganics and 900 °C, with partial or total volatilization of K, Cl and Na. This is in accordance with the mass loss measured with the TGA in this temperature range (Fig. 1). In addition, due to their different initial composition, each plant exhibits a specific behavior.

The most striking difference is the volatilization of K, which at 900 °C reaches 100%, 41.9% and 43.1% for *Rinorea*, *Alyssum* and *Leptoplax*, respectively. K volatilizes mainly into the compound KCl(g) and its dimer $(KCl)_2$(g) (from about 550 °C) and, to a lesser extent and at a higher temperature, as KOH(g). It can be noted that the experimental data related to K release are in rather good accordance with simulations.

Similarly to K, the behavior of Na depends on the plant, with complete volatilization as NaCl(g) around 600–700 °C for *Leptoplax* and *Rinorea*, while it is almost negligible for *Alyssum*. However, the amount of Na in the 3 HAs is much lower than K (mass ratio Na/K from1/60 to 1/20) and therefore does not have a significant influence on the total ash content.

The behavior of Cl at 500 °C is very different between the 3 HAs, without volatilization for *Alyssum*, while a significant amount of HCl(g) is formed for *Leptoplax* and *Rinorea*. At higher temperature, Cl volatilizes completely for each plant (at 650 °C for *Leptoplax* and *Rinorea* and at 850 °C for *Alyssum*). Cl is mainly involved in HCl(g), NaCl(g) and KCl(g).

Finally, S remains mainly in condensed phases, such as the compounds K_2SO_4 and $CaSO_4$ (Table 2), with a slight volatilization above 800 °C as SO_2(g) (Fig. 6d).

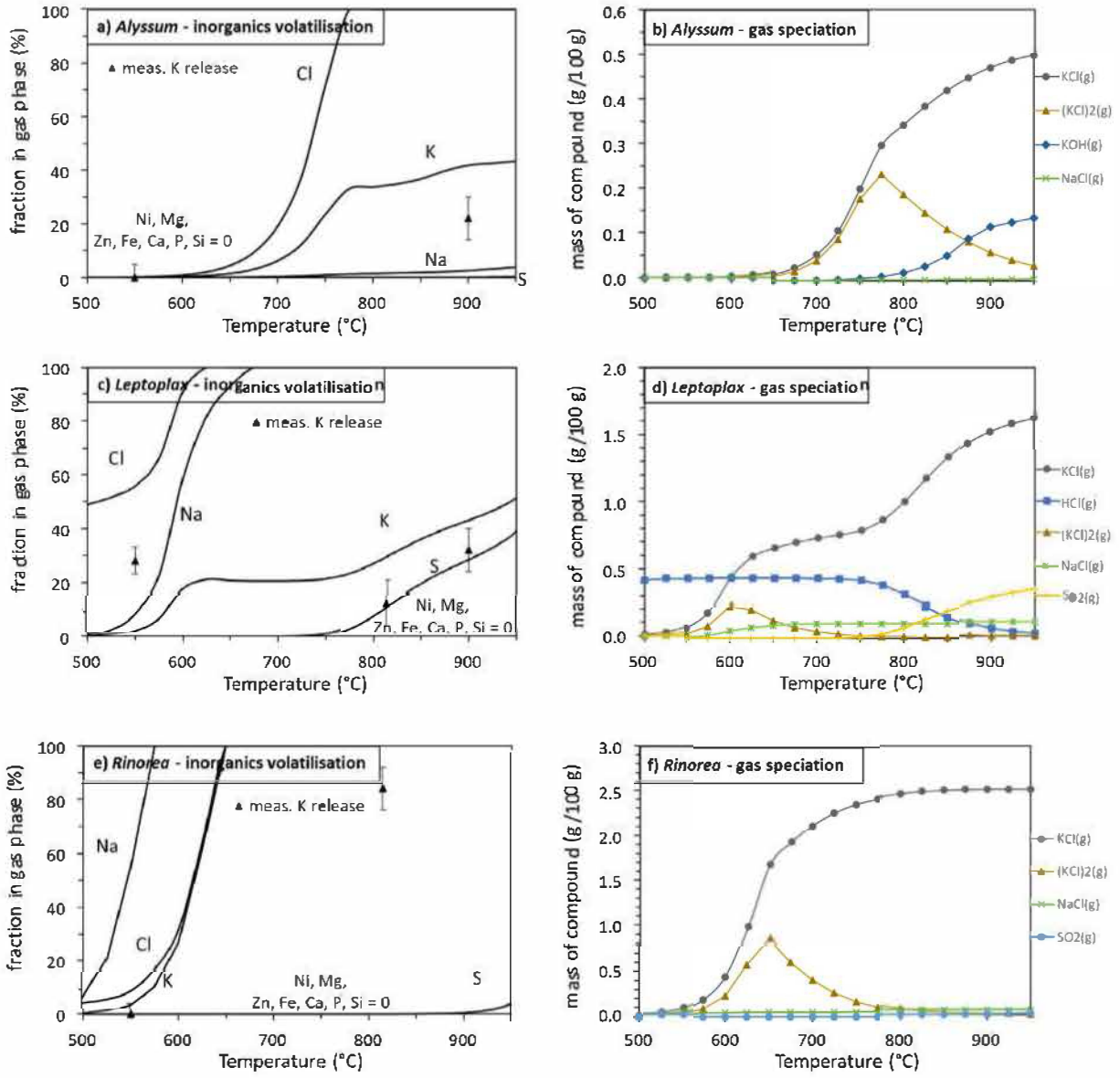

Fig. 6 – Influence of temperature on the volatilization of inorganic elements and speciation of the gas phase for *Alyssum* (a and b), *Leptoplax* (c and d) and *Rinorea* (e and f).

4. Discussion

The thorough comparison between the experimental data and the calculations presented in Section 3 demonstrates the overall relevance of simulation, which satisfactorily reproduces the mass variation, phase distribution and elemental composition of ashes and provides a clear picture of the behavior of inorganics during HA combustion.

Regarding the behavior of nickel, we show that this element fully stays in ashes and does not form any volatile compound during combustion, which is consistent with current knowledge related to the combustion of various biomass sources containing high levels of heavy metals (Nzihou and Stanmore, 2013). Furthermore, Ni is present in ashes as a single phase of nickel oxide (NiO) or in a mixture with MgO (Ni,Mg)O, as shown by the combination of analyses (XRD and SEM-EDX in Figs. 2 and 3) and calculations (Table 2). This behavior is independent of the initial plant composition as well as the temperature of combustion. The good match between simulation and ash analyses indicates that, at 900 °C, equilibrium is reached and reactions leading to the formation of the (Ni,Mg)O solid solution (in accordance with the NiO-MgO phase diagram), take place within the solid particles.

Despite the overall good agreement, there is an important discrepancy between the experimental ash yields measured after furnace combustion and simulations (Fig. 1). Indeed, our calculations systematically underestimate the ash yields, with a mean relative difference of −22% (σ = 7.8%) for 7 experimental data (Table 1). Among the volatile elements, the amount of S in the ashes is well reproduced by our simulations (Fig. 4), and thus it should not account for large mass differences. The most likely explanation is that our calculations do not well reproduce the amount of carbonate compounds in the ashes. Indeed, as illustrated in Fig. 5, there is a large difference between the calculated amount of carbon and the experimental value, and we noticed from XRD that $CaCO_3$ is present in *Alyssum* ashes while it is not foreseen in calculations (Table 2). If we attribute carbon atoms to CO_2 molecules (which corresponds to 3.62 g per g of carbon), the difference of carbon content between calculations

Table 3 – Initial molar content (in mol per 100 g of biomass) and molar ratio of selected inorganic elements for the three HA plants.

	K	Si	Cl	S	K/Cl	Si/K
Alyssum	2.24E−02	7.58E−03	7.28E−03	4.90E−03	3.40	3.39E−01
Leptoplax	5.07E−02	8.15E−03	2.40E−02	2.01E−02	2.18	1.61E−01
Rinorea	3.40E−02	6.20E−03	3.66E−02	9.30E−03	0.95	1.82E−01

and ashes accounts for about 15% at 550 °C and 4% at 900 °C of the mass difference. This could be due to calculation errors caused by insufficient description of the NiO-K_2O and CaO-K_2O systems in the database, leading to inaccurate prediction of the carbonate phases stability. Furthermore, despite specific precautions taken during ash yield measurements (combustion in dry synthetic air, cooling in desiccator as described in Section 2.3), small amounts of CO_2 or water might account for a mass gain in ashes due to reaction with atmosphere.

Apart from the behavior of nickel, which is very specific to our selection of HA plants, it can be noted that our results are in line with general knowledge regarding inorganics behavior during biomass combustion. Indeed, as described for instance in Koppejan and van Loo (2012), almost no volatilization of inorganics occurs at low temperature (typically 500–550 °C), and KCl, KOH and HCl are the major volatile compounds evolving in the 600–900 °C temperature range, accounting for a noticeable mass loss of the solid residue. In addition, thanks to the large differences in the 3 HA composition (Table 1), our results show that the release of K, Na and, to a minor extent, S, strongly depends on the initial inorganics content of the biomass, which is also fully in line with the state of the art. This behavior can be discussed with the light of various so-called *fuel indexes*, that have been reviewed and developed for instance by Sommersacher et al. (2012). Based on statistical correlations established for the combustion of 12 different biomass fuels, the authors evaluate the release of inorganic compounds depending on the initial composition of the biomass. The authors show that the Cl release does not strongly depend upon fuel composition and is usually in the range of >90 wt%, which is in line with our calculations for the 3 HA plants (Fig. 6). They also deeply discuss the K release and conclude that a high Si/K molar ratio leads to a preferred formation of potassium silicates that are bound in the bottom ash and therefore reduce the K release. Such behavior was recently confirmed by Feldmeier et al. (2019). However, for low Si/K ratios (<2.5), no clear correlation can be made. In our case, Si/K ratios (Table 3) are very low (<0.4), and thus such index is of no use to predict K release. It can also be noted that Sommersacher et al. report typical value for K release comprised between 10% and 30%, which is in line with our measurements and calculations for *Alyssum* and *Leptoplax* (Fig. 6). On the opposite, we found out that *Rinorea* exhibits a very high K release, with a good agreement between calculations (100% at $T > 650$ °C) and measurements (83% at 815 °C). This is likely to be attributed to the very low and rather unusual initial K/Cl ratio (<1) in *Rinorea* (Table 3). Finally, the authors also discuss the use of a $(K + Na)/[x(2S + Cl)]$ index to predict the gaseous emissions of SO_x and HCl, but the index requires preliminary data to evaluate the specific value of x for each biomass: this method was not applicable to our case.

5. Conclusions

In this work, we present the first application of thermodynamic calculations to evaluate the behavior of inorganic elements during the combustion of nickel HA plants, which is of importance in the development of the entire process chain for the recovery of Ni compounds. Combined with the experimental data acquired after isothermal combustion of three different plants, all the results allow us to draw several original conclusions.

From a methodological point of view, our work confirms that, using commercial databases and software, equilibrium calculation is a powerful approach to evaluate the behavior of inorganic elements in the thermal treatment of biomass, and provide an accurate picture of the nature and respective amount of the phases composing combustion residues. Compared to "simple" rules based on fuel indexes, equilibrium calculations provide a much more accurate tool to determine the overall inorganics behavior and the release of volatile elements. A discrepancy concerns the final amount of ash that is systematically underestimated by about 20–25% by our calculations, attributed to differences in the final carbonate content. This might be due to the still incomplete database description for the multi-element system composed by the HA plants. Indeed, the main inorganic sub-system for our HA plants is CaO–NiO–K_2O, and the current databases do not cover NiO–K_2O and CaO–K_2O subsystems, which could lead to inaccurate representation of CaO stability, and thus of $CaCO_3$ formation.

For the specific case of HA plants, an innovative result of this study is that, after combustion, nickel is always in the form of NiO particles, that can mix with MgO to form (Ni,Mg)O solid solutions. This result could not be deduced from the standard XRD analysis, and required a specific local elemental analysis guided by equilibrium calculations.

The better understanding of the behavior of some of the main inorganic elements has direct application to the understanding of the combustion process as well as to a better design of the subsequent leaching process, which consists of dissolving the ash in an acidic medium.

Funding

This work was supported by the EU LIFE-AGROMINE project (LIFE15 ENV/FR/000512); we gratefully acknowledge for this support.

Acknowledgments

We gratefully acknowledge our colleagues, Pr A. Bani (UAT, Tirana, Albania), Dr P. Kidd (CSIC, Santiago de Compostela, Spain), Pr J.-L. Morel (Université de Lorraine, Nancy, France) for providing the HA plants. The support of M.-L. de Solan

Bethmale for SEM-EDX analysis (LGC, Toulouse) was greatly appreciated.

Appendix A. Supplementary data

Supplementary data associated with this article can be found, in the online version, at https://doi.org/10.1016/j.cherd.2020.06.003.

References

Bale, C.W., Bélisle, E., Chartrand, P., Decterov, S.A., Eriksson, G., Gheribi, A.E., Hack, K., Jung, I.-H., Kang, Y.-B., Melançon, J., Pelton, A.D., Petersen, S., Robelin, C., Sangster, J., Spencer, P., Van Ende, M.-A., 2016. FactSage thermochemical software and databases, 2010–2016. Calphad 54, 35–53, http://dx.doi.org/10.1016/j.calphad.2016.05.002.

Bani, A., Pavlova, D., Echevarria, G., Mullaj, A., Reeves, R.D., Morel, J.-L., Sulçe, S., 2010. Nickel hyperaccumulation by the species of Alyssum and Thlaspi (Brassicaceae) from the ultramafic soils of the Balkans. Bot. Serbica 34 (1), 3–14.

Bani, A., Echevarria, G., Sulçe, S., Morel, J.L., 2015. Improving the agronomy of *Alyssum murale* for extensive phytomining: a five-year field study. Int. J. Phytoremediation 17, 117–127, http://dx.doi.org/10.1080/15226514.2013.862204.

Barbaroux, R., Meunier, N., Mercier, G., Taillard, V., Morel, J.L., Simonnot, M.O., Blais, J.F., 2009. Chemical leaching of nickel from the seeds of the metal hyperaccumulator plant *Alyssum murale*. Hydrometallurgy 100, 10–14, http://dx.doi.org/10.1016/j.hydromet.2009.09.005.

Barbaroux, R., Mercier, G., Blais, J.F., Morel, J.L., Simonnot, M.O., 2011. A new method for obtaining nickel metal from the hyperaccumulator plant *Alyssum murale*. Sep. Purif. Technol. 83, 57–65, http://dx.doi.org/10.1016/j.seppur.2011.09.009.

Barbaroux, R., Plasari, E., Mercier, G., Simonnot, M., Morel, J., Blais, J., 2012. A new process for nickel ammonium disulfate production from ash of the hyperaccumulating plant *Alyssum murale*. Sci. Total Environ. 423, 111–119.

Becidan, M., Sørum, L., Frandsen, F., Pedersen, A.J., 2009. Corrosion in waste-fired boilers: a thermodynamic study. Fuel 88, 595–604, http://dx.doi.org/10.1016/j.fuel.2008.10.032.

Chaney, R.L., Baker, A.J.M., Morel, J.L., 2018. The long road to developing agromining/phytomining. In: Van der Ent, A., Echevarria, G., Baker, A.J.M., Morel, J.L. (Eds.), Agromining: Farming for Metals: Extracting Unconventional Resources Using Plants. Springer International Publishing, Cham, pp. 1–17, http://dx.doi.org/10.1007/978-3-319-61899-9_1.

Feldmeier, S., Wopienka, E., Schwarz, M., Schön, C., Pfeifer, C., 2019. Applicability of fuel indexes for small-scale biomass combustion technologies, Part 2: TSP and NO_x emissions. Energy Fuels 33, 11724–11730, http://dx.doi.org/10.1021/acs.energyfuels.9b02589.

Froment, K., Defoort, F., Bertrand, C., Seiler, J.M., Berjonneau, J., Poirier, J., 2013. Thermodynamic equilibrium calculations of the volatilization and condensation of inorganics during wood gasification. Fuel 107, 269–281, http://dx.doi.org/10.1016/j.fuel.2012.11.082.

Guilpain, M., Laubie, B., Zhang, X., Morel, J.L., Simonnot, M.-O., 2018. Speciation of nickel extracted from hyperaccumulator plants by water leaching. Hydrometallurgy 180, 192–200.

Hazotte, C., Laubie, B., Pacault, S., Dufaud, O., Simonnot, M.O., 2019. Potential appraisal of nickel hyperaccumulator plants as combustion fuel. Biomass Bioenergy (submitted for publication).

Houzelot, V., Laubie, B., Pontvianne, S., Simonnot, M.-O., 2017. Effect of up-scaling on the quality of ashes obtained from hyperaccumulator biomass to recover Ni by agromining. Chem. Eng. Res. Des. 120, 26–33, http://dx.doi.org/10.1016/j.cherd.2017.02.002.

Kaknics, J., Defoort, F., Poirier, J., 2015. Inorganic phase transformation in Miscanthus ash. Energy Fuels 29, 6433–6442, http://dx.doi.org/10.1021/acs.energyfuels.5b01189.

Kangas, P., Koukkari, P., Hupa, M., 2014. Modeling biomass conversion during char gasification, pyrolysis, and torrefaction by applying constrained local thermodynamic equilibrium. Energy Fuels 28, 6361–6370, http://dx.doi.org/10.1021/ef501343d.

Kidd, P., Mench, M., Álvarez-López, V., Bert, V., Dimitriou, I., Friesl-Hanl, W., Herzig, R., Janssen, J.O., Kolbas, A., Müller, I., Neu, S., Renella, G., Ruttens, A., Vangronsveld, J., Puschenreiter, M., 2015. Agronomic practices for improving gentle remediation of trace element-contaminated soils. Int. J. Phytoremediation 17, 1005–1037, http://dx.doi.org/10.1080/15226514.2014.1003788.

Kidd, P.S., Bani, A., Benizri, E., Gonnelli, C., Hazotte, C., Kisser, J., Konstantinou, M., Kuppens, T., Kyrkas, D., Laubie, B., Malina, R., Morel, J.-L., Olcay, H., Pardo, T., Pons, M.-N., Prieto-Fernández, Á., Puschenreiter, M., Quintela-Sabarís, C., Ridard, C., Rodríguez-Garrido, B., Rosenkranz, T., Rozpadek, P., Saad, R., Selvi, F., Simonnot, M.-O., Tognacchini, A., Turnau, K., Wazny, R., Witters, N., Echevarria, G., 2018. Developing sustainable agromining systems in agricultural ultramafic soils for nickel recovery. Front. Environ. Sci. 6, http://dx.doi.org/10.3389/fenvs.2018.00044.

Konttinen, J., Backman, R., Hupa, M., Moilanen, A., Kurkela, E., 2013. Trace element behavior in the fluidized bed gasification of solid recovered fuels – a thermodynamic study. Fuel 106, 621–631, http://dx.doi.org/10.1016/j.fuel.2012.10.009.

Koppejan, J., van Loo, S., 2012. The Handbook of Biomass Combustion and Co-firing. Routledge.

Lindberg, D., Backman, R., Chartrand, P., Hupa, M., 2013. Towards a comprehensive thermodynamic database for ash-forming elements in biomass and waste combustion—current situation and future developments. Fuel Process. Technol. 105, 129–141, http://dx.doi.org/10.1016/j.fuproc.2011.08.008.

Ma, C., Backman, R., Öhman, M., 2015. Thermochemical equilibrium study of slag formation during pressurized entrained-flow gasification of woody biomass. Energy Fuels 29, 4399–4406, http://dx.doi.org/10.1021/acs.energyfuels.5b00889.

Nordgren, D., Hedman, H., Padban, N., Boström, D., Öhman, M., 2013. Ash transformations in pulverised fuel co-combustion of straw and woody biomass. Fuel Process. Technol. 105, 52–58, http://dx.doi.org/10.1016/j.fuproc.2011.05.027.

Nzihou, A., Stanmore, B., 2013. The fate of heavy metals during combustion and gasification of contaminated biomass—a brief review. J. Hazard. Mater. 256–257, 56–66, http://dx.doi.org/10.1016/j.jhazmat.2013.02.050.

Pardo, T., Rodríguez-Garrido, B., Saad, R.F., Soto-Vázquez, J.L., Loureiro-Viñas, M., Prieto-Fernández, Á., Echevarria, G., Benizri, E., Kidd, P.S., 2018. Assessing the agromining potential of Mediterranean nickel-hyperaccumulating plant species at field-scale in ultramafic soils under humid-temperate climate. Sci. Total Environ. 630, 275–286, http://dx.doi.org/10.1016/j.scitotenv.2018.02.229.

Pelton, A.D., Chartrand, P., 2001. The modified quasi-chemical model: Part II. Multicomponent solutions. Metall. Mater. Trans. A 32, 1355–1360, http://dx.doi.org/10.1007/s11661-001-0226-3.

Reeves, R.D., Baker, A.J.M., Jaffré, T., Erskine, P.D., Echevarria, G., van der Ent, A., 2018. A global database for plants that hyperaccumulate metal and metalloid trace elements. New Phytol. 218, 407–411, http://dx.doi.org/10.1111/nph.14907.

Rodrigues, J., Houzelot, V., Ferrari, F., Echevarria, G., Laubie, B., Morel, J.-L., Simonnot, M.-O., Pons, M.-N., 2016. Life cycle assessment of agromining chain highlights role of erosion control and bioenergy. J. Clean. Prod. 139, 770–778, http://dx.doi.org/10.1016/j.jclepro.2016.08.110.

Said, M., Cassayre, L., Dirion, J.-L., Joulia, X., Nzihou, A., 2017. On the relevance of thermodynamics to predict the behaviour of inorganics during CO_2 gasification of willow wood. In: Espuña, A., Graells, M., Puigjaner, L. (Eds.), Computer Aided Chemical Engineering. Elsevier, pp. 2671–2676, http://dx.doi.org/10.1016/B978-0-444-63965-3.50447-5.

Said, M., Cassayre, L., Dirion, J.-L., Nzihou, A., Joulia, X., 2018. Influence of nickel on biomass pyro-gasification: coupled thermodynamic and experimental investigations. Ind. Eng. Chem. Res. 57, 9788–9797, http://dx.doi.org/10.1021/acs.iecr.7b05201.

Sommersacher, P., Brunner, T., Obernberger, I., 2012. Fuel indexes: a novel method for the evaluation of relevant combustion properties of new biomass fuels. Energy Fuels 26, 380–390, http://dx.doi.org/10.1021/ef201282y.

Stam, A.F., Brem, G., 2019. Fouling in coal-fired boilers: biomass co-firing, full conversion and use of additives – a thermodynamic approach. Fuel 239, 1274–1283, http://dx.doi.org/10.1016/j.fuel.2018.11.127.

Thevenin, G., Poirier, J., Prigent, P., Fourcault, A., Robert-Arnouil, J.P., Edme, E., Marias, F., Demarthon, R., 2014. Modelling and design of a refractory lining for a biomass gasification reactor fed by a plasma torch. Waste Biomass Valor. 5, 865–877, http://dx.doi.org/10.1007/s12649-014-9292-9.

van der Ent, A., Baker, A.J.M., Reeves, R.D., Chaney, R.L., Anderson, C.W.N., Meech, J.A., Erskine, P.D., Simonnot, M.-O., Vaughan, J., Morel, J.L., Echevarria, G., Fogliani, B., Rongliang, Q., Mulligan, D.R., 2015. Agromining: farming for metals in the future? Environ. Sci. Technol. 49, 4773–4780, http://dx.doi.org/10.1021/es506031u.

van der Ent, A., Callahan, D.L., Noller, B.N., Mesjasz-Przybylowicz, J., Przybylowicz, W.J., Barnabas, A., Harris, H.H., 2017. Nickel biopathways in tropical nickel hyperaccumulating trees from Sabah (Malaysia). Sci. Rep. 7, 1–21, http://dx.doi.org/10.1038/srep41861.

Van der Ent, A., Echevarria, G., Baker, A.J.M., Morel, J.L. (Eds.), 2018. Agromining: Farming for Metals. Springer International Publishing, Cham, http://dx.doi.org/10.1007/978-3-319-61899-9_2.

Vassilev, S.V., Baxter, D., Andersen, L.K., Vassileva, C.G., 2013. An overview of the composition and application of biomass ash. Part 1. Phase – mineral and chemical composition and classification. Fuel 105, 40–76, http://dx.doi.org/10.1016/j.fuel.2012.09.041.

Wan, W., Engvall, K., Yang, W., 2018. Novel model for the release and condensation of inorganics for a pressurized fluidized-bed gasification process: effects of gasification temperature. ACS Omega 3, 6321–6329, http://dx.doi.org/10.1021/acsomega.8b00019.

Xing, P., Darvell, L.I., Jones, J.M., Ma, L., Pourkashanian, M., Szuhánszki, J., Williams, A., 2018. The use of equilibrium thermodynamic models for the prediction of inorganic phase changes in the co-firing of wheat straw with El Cerrejon coal. J. Energy Inst., http://dx.doi.org/10.1016/j.joei.2018.02.003.

Zeng, T., Weller, N., Pollex, A., Lenz, V., 2016. Blended biomass pellets as fuel for small scale combustion appliances: influence on gaseous and total particulate matter emissions and applicability of fuel indices. Fuel 184, 689–700, http://dx.doi.org/10.1016/j.fuel.2016.07.047.

Zhang, X., Houzelot, V., Bani, A., Morel, J.L., Echevarria, G., Simonnot, M.-O., 2014. Selection and combustion of Ni-hyperaccumulators for the phytomining process. Int. J. Phytoremediation 16, 1058–1072, http://dx.doi.org/10.1080/15226514.2013.810585.